# Synthesis of Layered Silicon-Graphene Hetero-structures by Wet Jet Milling for High Capacity Anodes in Li-ion Batteries

Romeo Malik,[1] Qianye Huang,[1] Laura Silvestri,[2,3] Danqing Liu,[1] Vittorio Pellegrini,[3,4] Luigi Marasco,[3] Eleonora Venezia,[3] Sara Abouali[3], Francesco Bonaccorso,[3,4] Michael J. Lain,[1] David Greenwood,[1] Geoff West,[1] Paul R. Shearing,[5] and Melanie J. Loveridge*[1]

[1]*WMG, University of Warwick, Gibbet Hill Road, Coventry, CV4 7AL.*

[2]*Dipartimento di Tecnologie Energetiche, ENEA C.R Casaccia, via Anguillarese 301, Rome, 00123 Italy*

[3]*Graphene Labs Istituto Italiano di Tecnologia, Via Morego 30, Genova, 16163 Italy*

[4]*Bedimensional Spa, Via Albisola 121, Genova, 16163, Italy*

[5]*The Electrochemical Innovation Lab, Department of Chemical Engineering, University College London, Torrington Place, London WC1E 7JE, UK*

**Corresponding Author:** Melanie J. Loveridge (M.Loveridge@warwick.ac.uk)

## Supplementary Figures

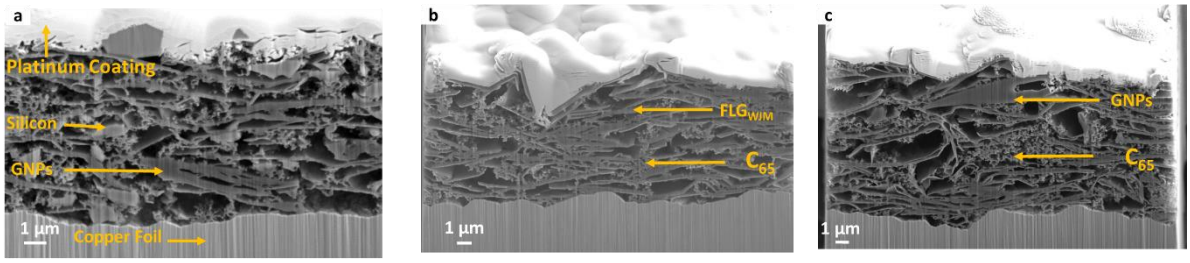


**Figure S1:** Cross-sectional images of electrode with (a) Formulation D - composite nm Si with FLG$_{WJM}$, (b) Formulation E - FLG$_{WJM}$ dominant, and (c) Formulation F - GNPs dominant powders.

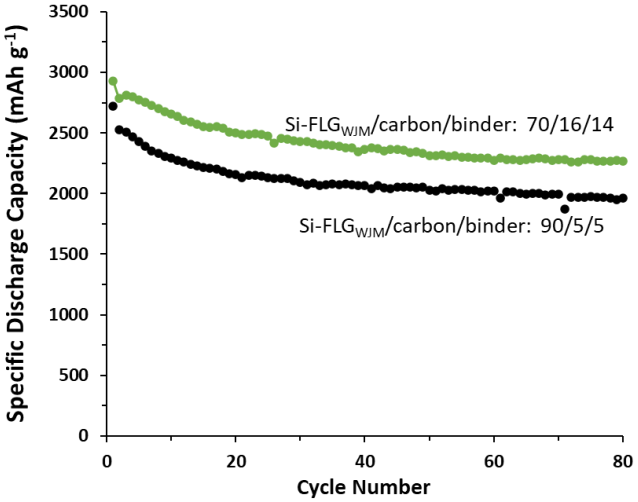


**Figure S2:** Comparison the cyclic performances of Si-FLG$_{WJM}$ electrodes with different amounts of carbon and binder cycled at full capacity of silicon (3579 mAh g$^{-1}$).

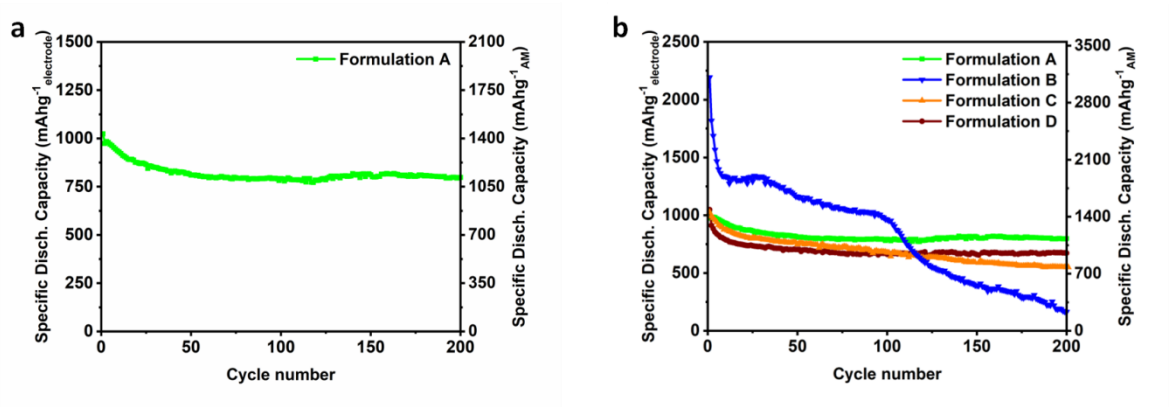


**Figure S3:** Specific discharge capacity as function of cycle number plot for (a) Formulation A and (b) comparison of cycling behaviour for Formulation A-D. The electrochemical measurements were conducted in lithium cell by galvanostatic cycling at 0.2C (1C = 3579 mA $g^{-1}$) in the voltage range 0.05-1V. First cycle has been carried out at C/20. In left Y axis is reported the specific capacity referred to the mass of the whole electrode (including active material, conductive carbon and binder). In the right y axis is reported the specific capacity referred to the mass of the active materials, i.e Si and/or graphene source.

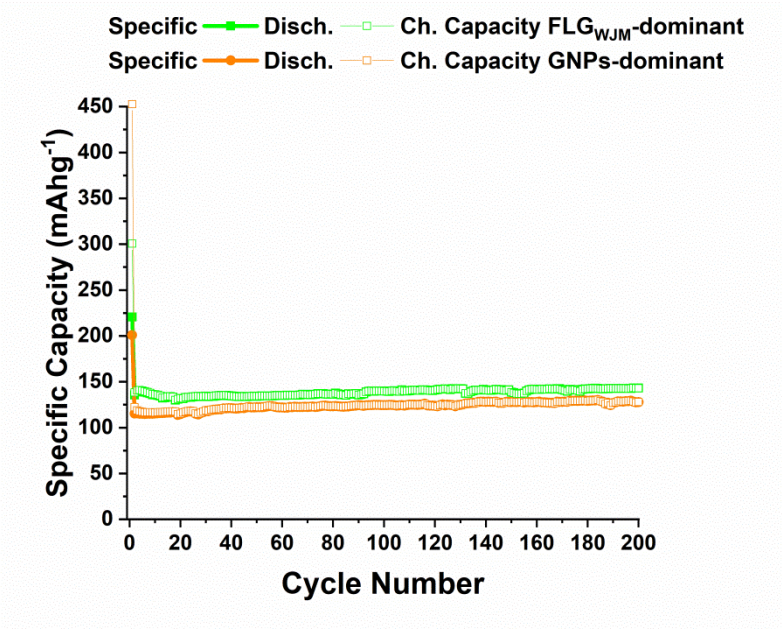


**Figure S4:** Specific capacity (based on the graphene's active mass) as function of cycle number plot for graphene dominant electrodes obtained by galvanostatic cycling at 0.2C (1C=3579 mA$g^{-1}$) in the voltage range 0.05-1V. First cycle has been carried out at C/20.

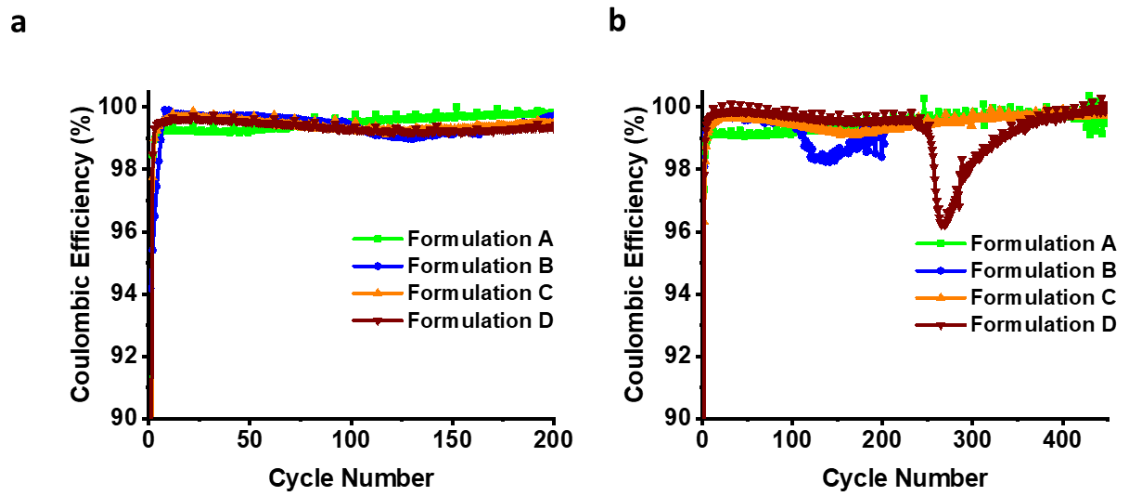


**Figure S5:** Coulombic Efficiency profiles of formulations cycled at (a) full capacity of silicon (3579 mAh $g^{-1}$) and (b) half capacity of silicon (1800 mAh $g^{-1}$).

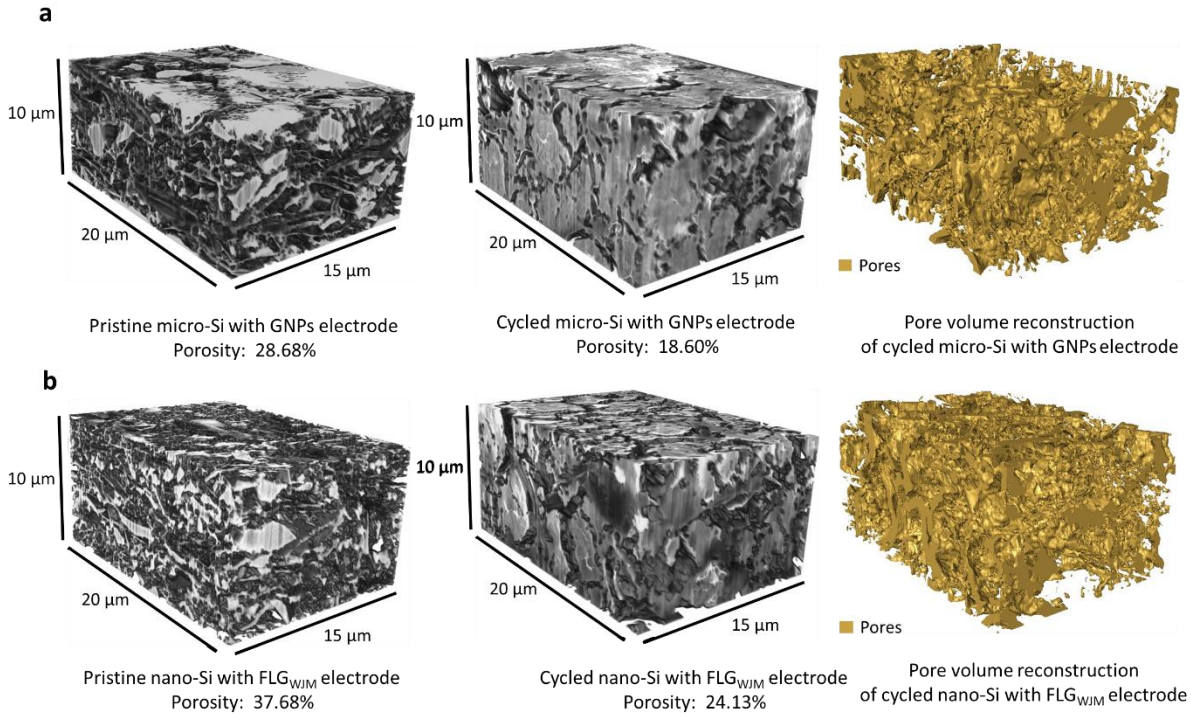


**Figure S6:** The greyscale 3D reconstructed volume of the electrode with (a) Formulation C - composite µm Si with GNP powders, (b) Formulation D - composite nm Si with $FLG_{WJM}$ powders, before and after cycling at full capacity for 200 cycles.

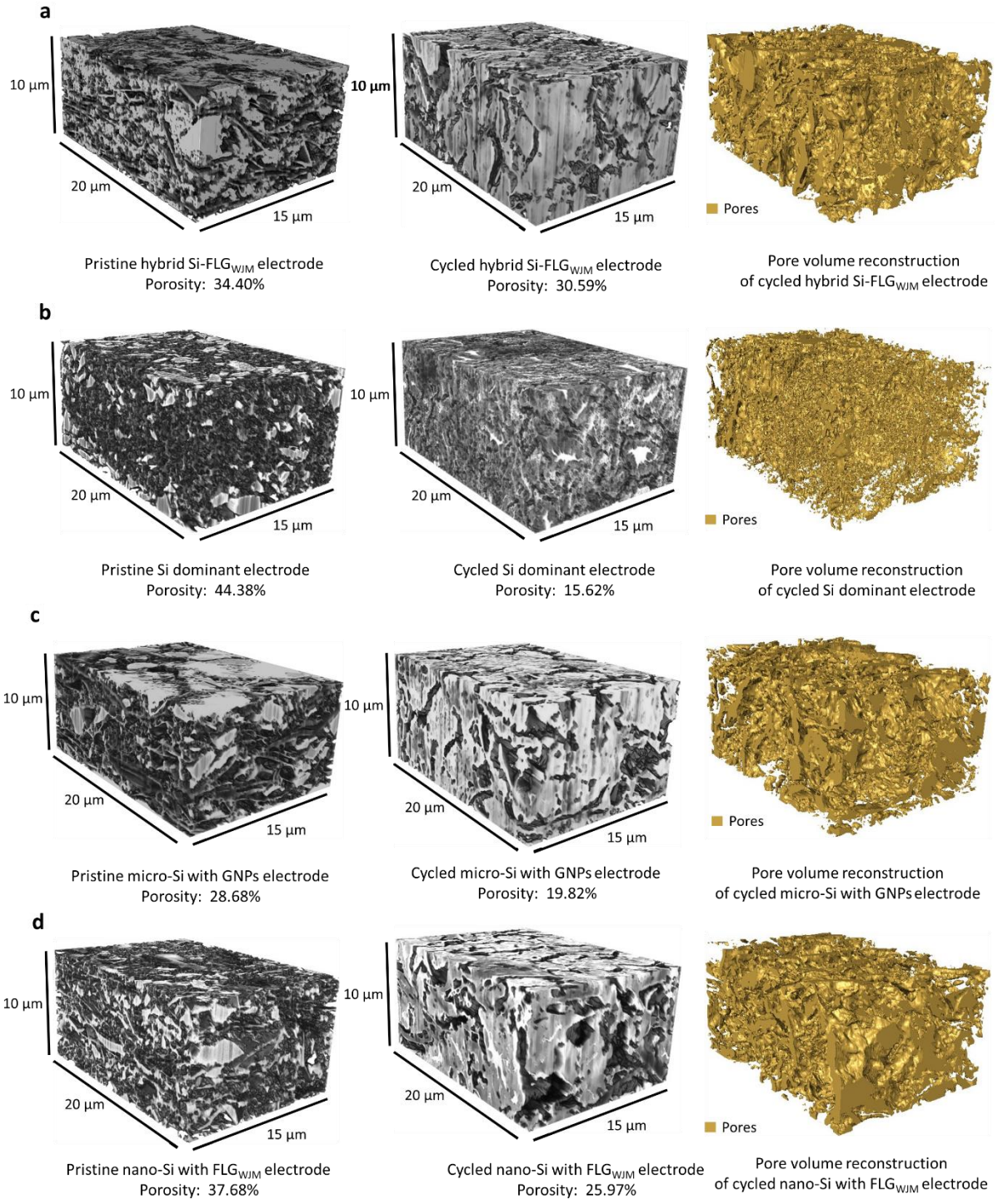


**Figure S7:** The greyscale 3D reconstructed volume of the electrode with (a) Formulation A - Si-FLG$_{WJM}$ composite, (c) Formulation B - Si-dominant, (c) Formulation C - composite µm Si with GNP powders, (d) Formulation D - composite nm Si with FLG$_{WJM}$ powders, before and after cycling at half capacity for 200 cycles.

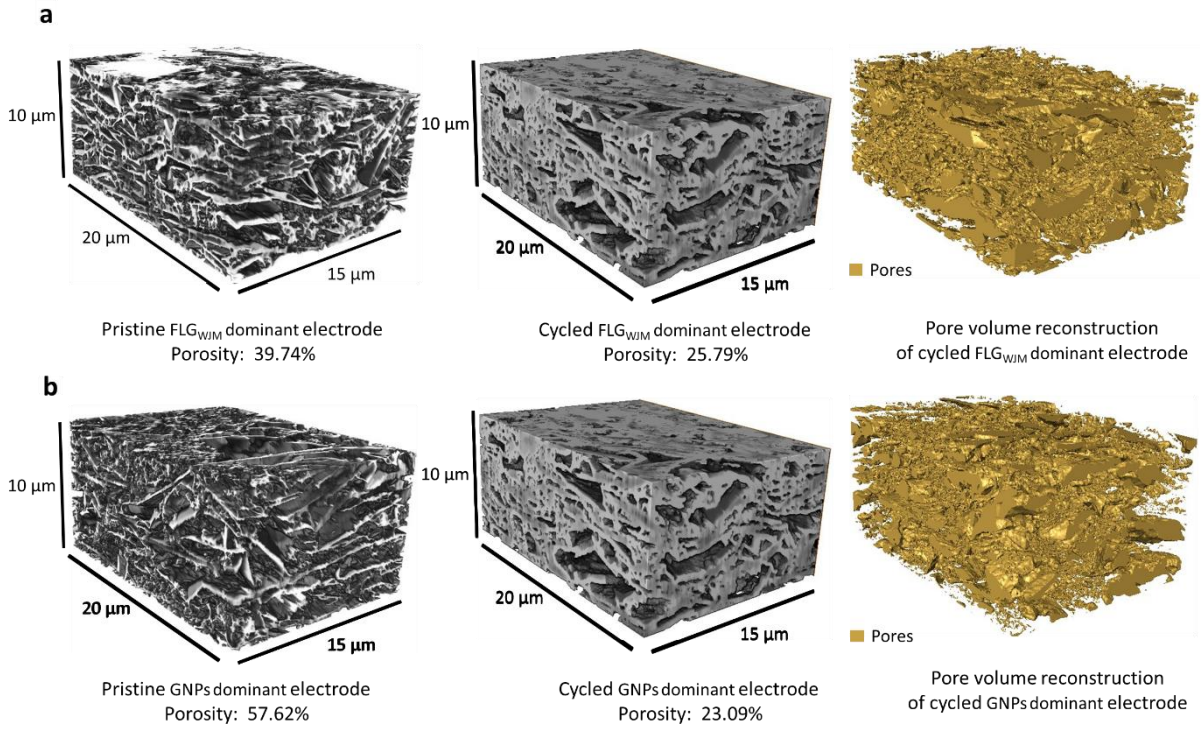


**Figure S8:** The greyscale 3D reconstructed volume of the electrode with (a) Formulation E - FLG$_{WJM}$ dominant, (b) Formulation F - GNPs dominant, before and after cycling for 200 cycles at the same current as applied to Formulation A - Si-FLG$_{WJM}$ composite.

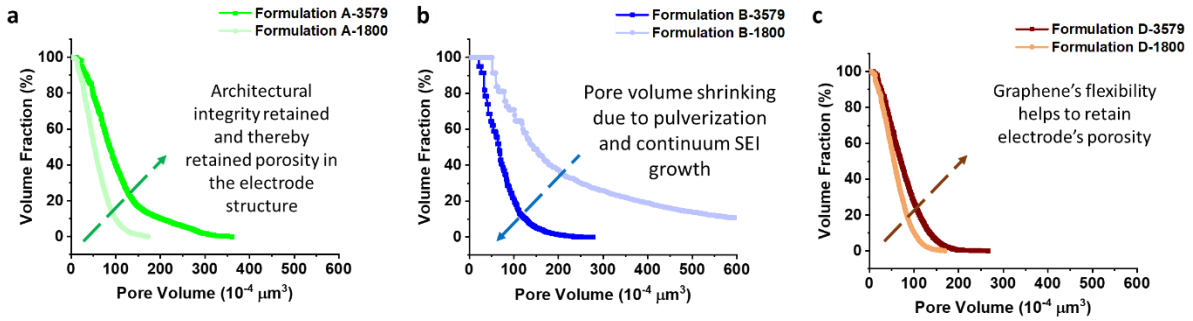


**Figure S9**: Cumulative pore volume distribution comparison after 200 cycles under half and full capacity of Si for (a) Formulation A, (b) Formulation B, (c) Formulation D.

## Supplementary Table

**Table S1:** Surface Area (SA) comparison for graphene dominant electrodes before after cycling at the same current as applied to Formulation A - Si-FLG$_{WJM}$ composite.

| Samples | SA – µm$^2$ | | SA – µm$^2$ (% change) |
|---|---|---|---|
| | Pristine | Cycled | Cycled |
| Formulation E | 1.01755e+10 | 7.8323e+09 | 23.03 % |
| Formulation F | 1.28485e+10 | 6.43731e+09 | 49.90 % |

**Table S2:** Electrode thickness (SA) comparison for graphene dominant electrodes before after cycling at the same current as applied to Formulation A - Si-FLG$_{WJM}$ composite.

| Samples | Thickness – µm | | Thickness – µm (% change) |
|---|---|---|---|
| | Pristine | Cycled | Cycled |
| Formulation E | 10.57 | 10.94 | -3.50 % |
| Formulation F | 11.49 | 12.64 | -10.01 % |

**Table S3:** Specifications of different electrodes.

| Samples | Thickness (µm) | Film bulk density (g/cm$^3$) |
|---|---|---|
| **Formulation A** | **11.88** | **1.06** |
| **Formulation B** | **11.33** | **1.50** |
| **Formulation C** | **10.95** | **1.00** |
| **Formulation D** | **15.13** | **1.10** |
| **Formulation E** | **10.57** | **1.28** |
| **Formulation F** | **11.49** | **1.27** |

**Supplementary Information**

## Material Characterisation

### Thermo-gravimetric analysis (TGA):

TGA was performed to determine the content of silicon within the Si-$FLG_{WJM}$ composite (see Fig. S10). The experiment was conducted in a TGA (Q500, TA Instrument) and the temperature scan comprised a run to 800 °C at 5 °C$min^{-1}$ followed by an isothermal step of 2 hours at 800 °C. The same program was used for a pristine silicon sample as a control comparison, with all the measurements carried out in air. Fig. S10 shows the thermograms obtained for the two samples. In the case of Si-$FLG_{WJM}$ composite powder, mass loss starts above 600 °C and at the end of the scan approximately 55.4 wt.% is lost. While, in the case of the only Si powder, the weight starts to rise above 300 °C due to the formation of $SiO_x$ species, acquiring the 10 % of weight at the end of the scan. From the analysis of the two curves, we calculated that the weight ratio between Si and $FLG_{WJM}$ in the composite is 54.6 and 45.4 respectively. The rough mass ratio (1:1) of Si to graphene in Si-$FLG_{WJM}$ can be estimated herein.

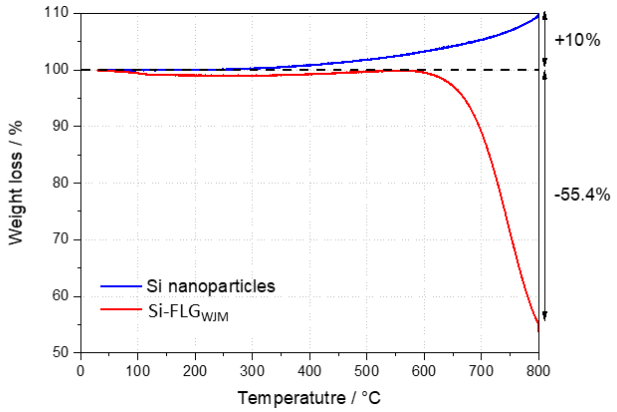


**Figure S10:** Thermogravimetric analysis of Si-$FLG_{WJM}$ composite and SiNPs heated at 800 °C in air-flow at 5 °C $min^{-1}$.

### Raman spectroscopy:

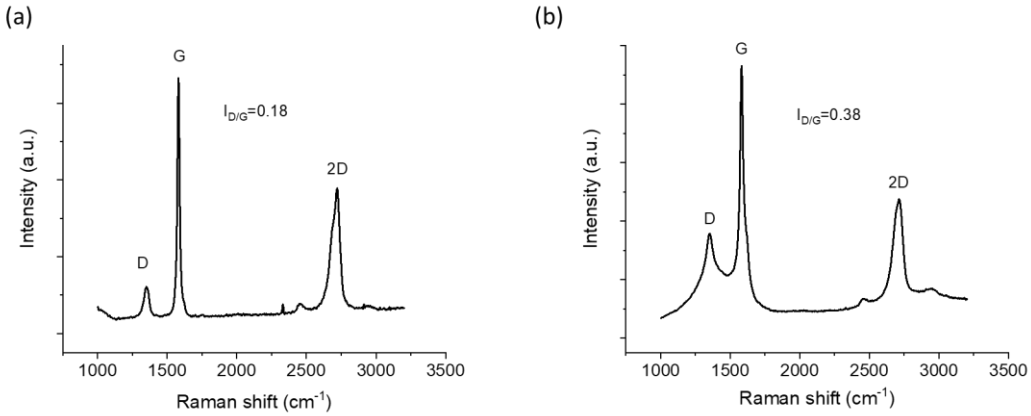


**Figure S11:** Raman spectrum of (a) $FLG_{WJM}$ and (b) the commercial GNPs.

The Raman spectrum of graphene-based materials shows four main peaks *i.e.*, G (~1585 $cm^{-1}$), D (~1380 $cm^{-1}$), D' (~1620 $cm^{-1}$) and 2D (~2700 $cm^{-1}$).[1,2] The G peak corresponds to the $E_{2g}$ phonon at the Brillouin zone centre. The D peak is due to the breathing modes of $sp^2$ rings, requiring a defect for its activation by double resonance.[3] The latter happens as an intra-valley process, *i.e.,* connecting two points belonging to the same cone around K or K', giving origin to the D' peak.[2,3] The 2D peak represents the second order of the D peak, being present also in the absence of D peak, since no defects are required for the activation of two phonons with the same momentum, one backscattered from the other.[2] Moreover, the 2D peak is an excitation wavelength-dependent single peak for graphene, whereas is a superposition of multiple components, the main being the $2D_1$ and $2D_2$ components, for few-layers graphene (FLG).[1] In graphite, the intensity of the $2D_2$ band is twice the one of the $2D_1$ band, while for graphene the 2D band is a single and sharp Lorentzian band, which is approximately four times more intense compared to the G peak.[2] Taking into account the intensity ratio between $2D_1$ and $2D_2$, it is possible to estimate the flake thickness.

To compare the quality of two kinds of graphene, the Raman spectra of $FLG_{WJM}$ and the commercial GNPs, were recorded at 532nm (Fig. S11). Using the ratio of peak intensities I(D)/I(G), the defect density of graphene can be estimated. The lower ratio of $FLG_{WJM}$ (0.18), compared to the one of commercial GNPs (0.38), indicates a higher graphene quality produced by the wet-jet milling procedure.

**Indentation Test**

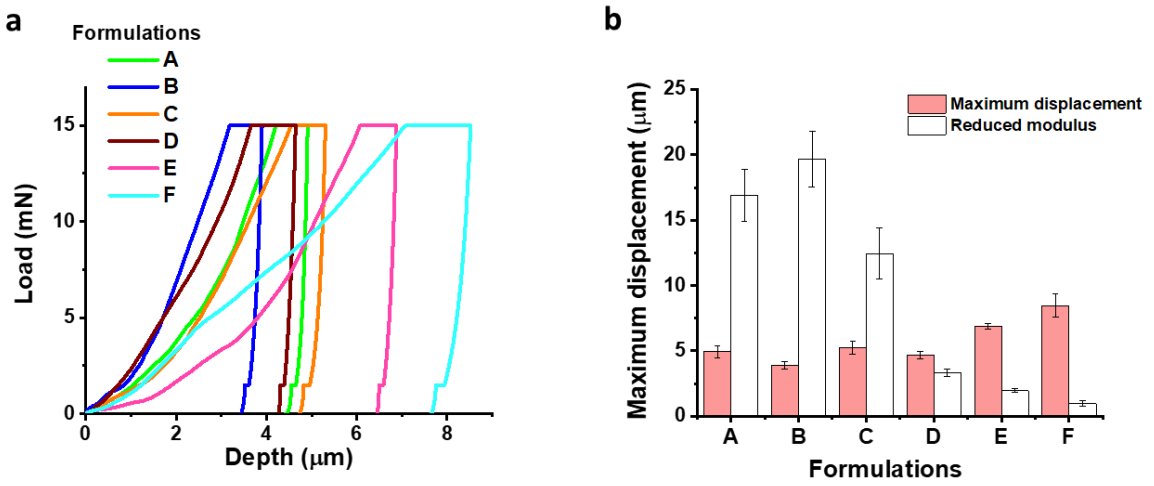


**Figure S12:** (a) Tensile curves and (b) maximum displacement, reduced Young's modulus deduced from nano-indentation tests.

It is believed that the highly conductive and flexible graphene sheets are suitable to form a buffer matrix to sustain Si particles' volume strain during lithiation/de-lithiation process.[4] To elucidate the above claim in our composite we performed nano-indentation testing to the prepared electrodes. The grid indentation procedure is a quick and reliable method to measure and compare composite electrodes for their mechanical properties[5,6]. Fig. S12a demonstrates the load-depth curve for all the samples including graphene dominant electrodes (Formulation E and F). The reduced elastic modulus is calculated using data taken from the slope of the tangent to the unloading curve. The results of the maximum depth and reduced modulus from unloading segment are shown in Figure S12b. It can be observed from Fig. S12b

that for graphene dominant electrodes, the tensile curves display a larger indentation depth and lower reduced modulus, indicating a more elastic property compared with the Si-$FLG_{WJM}$ composite. This is possible due to the larger the commercial GNPs flakes in comparison $FLG_{WJM}$, which also result to a larger pore size within the electrode. As a result, the μm sized Si-GNPs composite demonstrates larger contact depth and lower reduced modulus. Comparing Formulation A and D, the latter is a physically blended nm Si particles and as-synthesised graphene, it can be noted that the Formulation D shows similar contact depth but much lower reduced modulus. This might be due to more porosity introduced between nm Si and $FLG_{WJM}$ during the physical mixing and drying process, whilst in the Si-$FLG_{WJM}$ composite electrode, the SiNPs are firmly attached to graphene flakes. Therefore, we can postulate that the graphene provides an effective mechanical flexibility to accommodate volume expansion stresses from silicon upon cycling. In comparison to Formulation D, there is enhanced performance from maintaining the structural integrity of the electrode with Formulation A, as observed in cycling data in Fig. 2a, 2b and 2d.

**Representative Volume Element (RVE) Analysis:**

For reconstructing a statistically significant volume to compute geometrical parameters like porosity, pore surface area, and tortuosity, the largest possible cuboid volume was chosen as a region of interest across all the tomographic dataset. However, to ensure that the selected region of interest is a representative of the whole electrode, representative volume element (RVE) analysis was carried out for porosity as a geometrical parameter of interest. The electrode constituent's morphology and physical properties determine the size of RVE. In our study, this RVE was estimated by systematically analysing the influence of volume size on porosity as a parameter of interest (see Fig. S13). As seen from the Fig. S13, the minimum RVE is $18 \times 9 \times 15$ $\mu m^3$, as after this point the volume size has insignificantly influenced porosity and therefore it's seen as a distinctive flat distinct plateau. The change in porosity after this point was less than 0.5 %. However, for better representation of the bulk electrode, we analysed the whole $20 \times 10 \times 15$ $\mu m^3$ volume.

**Table S4.** The dimensions of sub-volumes of hybrid Si-FLG$_{WJM}$ electrodes analysed for representing the minimum RVE (RVE$_{min}$).

| Sample sub-volume ($V_n = x_n \cdot y_n \cdot z$) | x (µm) | y (µm) | z (µm) |
|---|---|---|---|
| $V_1$ | 2 | 1 | 15 |
| $V_2$ | 4 | 2 | 15 |
| $V_3$ | 6 | 3 | 15 |
| $V_4$ | 8 | 4 | 15 |
| $V_5$ | 10 | 5 | 15 |
| $V_6$ | 12 | 6 | 15 |
| $V_7$ | 14 | 7 | 15 |
| $V_8$ | 16 | 8 | 15 |
| $V_9$ | 18 | 9 | 15 |
| $V_{10}$ | 20 | 10 | 15 |

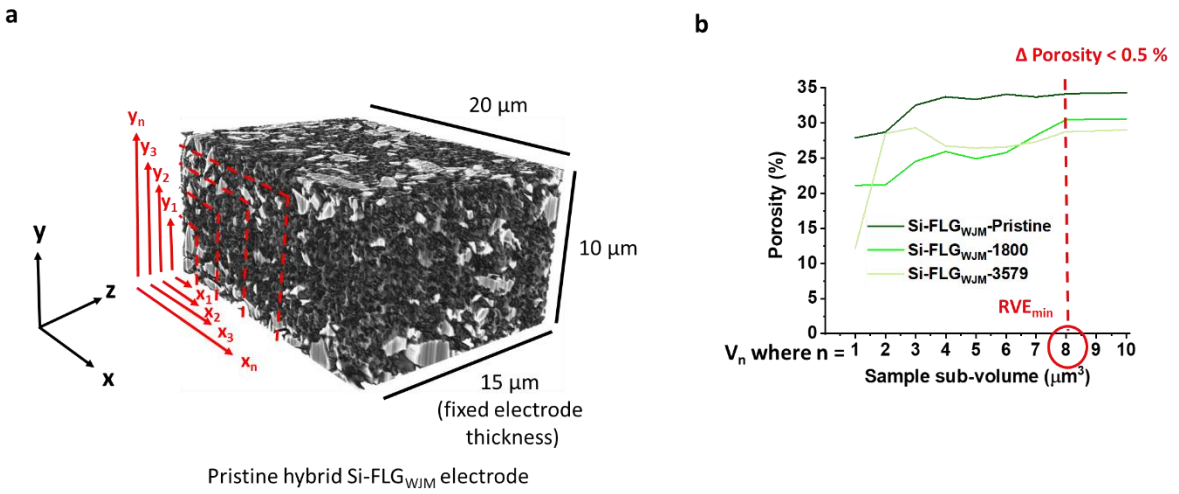


**Figure S13:** (a) Schematic representation of RVE analysis by increasing the electrode sub-volumes in x and y-direction and keeping the thickness fixed (z-direction), (b) Relationship between porosity and volume size and estimation of RVE$_{min}$.

## References

(1) Ferrari, A. C.; Meyer, J. C.; Scardaci, V.; Casiraghi, C.; Lazzeri, M.; Mauri, F.; Piscanec, S.; Jiang, D.; Novoselov, K. S.; Roth, S.; et al. Raman Spectrum of Graphene and Graphene Layers.

*Phys. Rev. Lett.* **2006**, *97* (18), 187401.

(2) Ferrari, A. C.; Basko, D. M. Raman Spectroscopy as a Versatile Tool for Studying the Properties of Graphene. *Nat. Nanotechnol.* **2013**, *8* (4), 235–246.

(3) Thomsen, C.; Reich, S. Double Resonant Raman Scattering in Graphite. *Phys. Rev. Lett.* **2000**, *85* (24), 5214–5217.

(4) Gan, L.; Guo, H.; Wang, Z.; Li, X.; Peng, W.; Wang, J.; Huang, S.; Su, M. A Facile Synthesis of Graphite/silicon/graphene Spherical Composite Anode for Lithium-Ion Batteries. *Electrochim. Acta* **2013**, *104*, 117–123.

(5) Vasconcelos, L. S. de; Xu, R.; Li, J.; Zhao, K. Grid Indentation Analysis of Mechanical Properties of Composite Electrodes in Li-Ion Batteries. *Extrem. Mech. Lett.* **2016**, *9*, 495–502.

(6) Huang, Q.; Loveridge, M. J.; Genieser, R.; Lain, M. J.; Bhagat, R. Electrochemical Evaluation and Phase-Related Impedance Studies on Silicon–Few Layer Graphene (FLG) Composite Electrode Systems. *Sci. Rep.* **2018**, *8* (1), 1386.